Journal of Applied Fluid Mechanics, Vol. 17, No. 4, pp. 726-741, 2024.
Available online at www.jafmonline.net, ISSN 1735-3572, EISSN 1735-3645.
https://doi.org/10.47176/jafm.17.4.2305

Dispersion and Phase Exchange Process of Chemically Reactive Solute Through Circular Tube

Jyoti[1], S. Kwak[2], S. Ham[2] and J. Kim[2†]

[1] *The Institute of Basic Science, Korea University, Seoul 02841, Republic of Korea*
[2] *Department of Mathematics, Korea University, Seoul, 02841, Republic of Korea*

†Corresponding Author Email: cfdkim@korea.ac.kr

ABSTRACT

This article explores how a chemically reactive solute will disperse across mobile to immobile phase when injected into the fluid flowing within a long circular tube. To model this process, we utilized mathematical modeling, including advection-diffusion equations for flow of fluid within the tube and first-order chemical reaction equations to account for reversible and irreversible reactions on the tubes' wall. We proposed a numerical method based on an explicit finite difference scheme to solve the governing equations for the dispersion of a chemically reactive solute. We used an upwind method with a conservative representation in the diffusion component to discretize the advection-diffusion equation. To ensure the stability of our proposed numerical scheme, we computed the time step constraint condition so that the maximum principle for the discrete governing equation holds. We also verified the performance of our proposed scheme through computational results that were compared with previous studies. One of our key findings was that the depletion coefficient D_0 achieved a quasi-steady state for larger absorption rates. We also observed that the advection coefficient D_1 initially increased with an increasing absorption rate, but eventually declined due to phase exchange kinetics. The dispersion coefficient D_2 also decreased with a rising absorption rate due to a low-velocity gradient in the middle region. Our study showed that rapid distributions are possible under certain conditions, such as a high Damköhler number ($Da \geq 10$) and a high absorption rate (Γ>5). Computational results show that the proposed scheme can be useful in developing an efficient pulmonary drug delivery system for periodic inhalation of drugs to determine the optimal frequency of injection.

Article History

Received September 11, 2023
Revised October 31, 2023
Accepted November 25, 2023
Available online January 30, 2024

Keywords:

Chemical reactions on Boundary wall
Diffusion
Phase exchange
Periodic drug delivery
Taylor dispersion

1. INTRODUCTION

Sir Geoffrey Ingra Taylor (1953) gave a theory of the distribution of chemically reactive solutes injected over a short time into a Newtonian liquid flowing longitudinally through a pipe with Poiseuille flow. His theory is applicable across various fields such as hydrology to find the dispersion of pollutants in rivers (Ani et al., 2009; Fu et al., 2016; Barati & Saghafian, 2022), chemistry for the process of chromatography (Giddings & Eyring, 2002; Shankar & Lenhoff, 1991; Bel Hadj Taher et al., 2022; Venditti et al., 2022), environment for wetland flow (Mazumder & Das, 1992;Wu et al., 2012; Yang et al., 2021), and so on. Numerous studies exist (Chatwin, 1970; Gill & Sakarasubramanian, 1970; Davidson & Schroter, 1983; Jiang & Grotberg, 1993; Wu & Chen, 2014; Paramanantham, et al. 2022), which have extended Taylors' theory of dispersion for different time approximations using analytical methods such as Aris (1956) used a method of moments to calculate large time dispersion of a gaseous solute after the initial injection inside the flow of fluid. Sankarasubramanian and Gill (1973) used the method of mean concentration expansion by adding phase exchange conditions to calculate the temporal variation in solute dispersion at all times. Wu and Chen (2014) used the homogenization technique and introduced a longitudinal correction function for finding the skewed distribution of transverse mean concentrations over a long-time scale. Rana and Murthy (2016) used the eigenfunction expansion method to find the coefficients of variation, transport coefficients and distribution coefficients in small- and large- time approaches. Additionally, Wang and Huai (2019) performed stochastic analysis to find the absorption probability of walls at an

NOMENCLATURE

Symbols	Description	Symbols	Description
$\boldsymbol{a}$	radius of circular tube	N_z	number of cells in z −direction
C	concentration of species	Pe	Peclet number
c_m	the center of mass	Δr	cell size in radial direction
$\bar{c}$	mean concentration of the mobile phase	R	radial distance
c_t	total mass of the mobile phase	Δt	time step
C_0	initial concentration	T	time
C_s	the concentration of species absorbed by the tube wall	V	axisymmetric velocity field
D_0	depletion coefficient	U	radial component of the velocity
D_1	dispersion coefficient	W	axial component of the velocity
D_2	advection coefficient	W_0	section-mean velocity
Da	Damköhler number indicates the kinetics of phase exchange.	Δz	cell size in axial direction
D	diffusion coefficient of species in the fluid	Z	axial distance
i	index for r −direction	Z_s	input length of the chemical solute
k	index for z −direction	α	phase partition coefficient
κ	reversible phase exchange rate	Γ	rate of solute absorbed irreversibly by the immobile phase
μ_n	axial moment of concentration distribution	σ	variance of the distribution
N_r	number of cells in r −direction	Ω	domain

early stage by utilizing a random walk particle tracking method. Recently, Jiang et al. (2022) provided an analytical method that can be used to calculate higher-order statistics including skewness and kurtosis across all ime scales. Therefore, consideration of time-dependent dispersion for long or short periods is an important factor. Moreover, several physiological processes can be understood by combining the initiative of Taylor dispersion with the theory of mean concentration distribution during transport processes, such as boundary uptake (Ng & Rudraiah, 2008), phase exchange (Kori & Pratibha, 2020; Wu et al., 2022), partitioning, energy uptake by cells, and binding of oxygen with hemoglobin (BEN-Tal, 2006). To address these processes inside the human body, the timeframe is as crucial as chemical reactions, retention, diffusion, and convection. Davidson and Schroter (1983) used Ariss' method of moments with reversible reaction to examine the dispersion of slug and axial velocity at different time periods through straight and thick-walled tubes. Jiang and Grotberg (1993) used a derivative-expansion method to find the dispersion of a contaminated solute in a straight tube with the consideration of an irreversible equation. While Rana and Murthy (2017) used extended convection-diffusion model to study the transient flow of blood from arteries of different diameters in the presence and absence of absorption. Moreover, many numerical attempts are also taken by focusing on these factors such as Ng and Rudraiah (2008) used reversible and irreversible reactions at the tube wall to calculate the advection and diffusion of chemical species through small diameter tubes (airways). They used a flux-corrected transport algorithm and solved the problem by using an explicit finite difference scheme with a condition for stability i.e., Courant number ≤0.5. A finite-difference implicit scheme with linear stability is used by Mazumder and Paul (2012) to analyze the dispersion of a chemical species through an annular tube with oscillatory walls. In continuation, Saini et al. (2014) extended the work of Ng and Rudraiah (2008) by including fluid reaction terms and solved the problem numerically using the explicit finite difference technique. Recently, Das et al. (2021) have investigated the influence of wall absorption on dispersion using the immersed boundary approach with staggered grids.

In the field of biomedical engineering to analyze the diffusing ability of drugs in the arterial blood, control release and at the targeted sites (Shaw et al., 2014; Das et al., 2021; Beg & Roy, 2022; Le & Tran, 2022; Mohseni & Domfeh, 2023) injection of solute (drug) in a frequent time is an important topic of research. However, several researchers have paid attention to the drug delivery system and contributed with different methods. Shaw et al. (2014) combined the numerical Fourier inversion approach with the Laplace transform methodology to look at how drug delivery works in nanoparticles. They stated that the design of nanoparticles affects the site of deposition. Ibrahim et al. (2013) used Taylor dispersion through a catheterized artery with an absorptive vascular system to assess the size of nanoparticles in the drug delivery system by using layer-adapted meshes and finite difference techniques. To study the dispersion of bi-component species within the blood flow Beg and Roy (2022) used a Crank-Nicolson implicit numerical scheme and predicted various results for drug transportation through confined vessels. To study the diffusion processes of a reactive species through a cardiovascular system a two-fluid model is used by Roy and Beg (2021) with low level of Peclet number (100). The researchers used analytical solutions to characterize the velocity distribution, as well as Gill's decomposition approach to evaluate the concentration profile with first-order chemical reaction and fixed axial pressure gradient. Additionally, a non-Newtonian Hershel-Bulkley fluid model is used by Abidin et al. (2021) to study the flow of blood through stenosed arteries under the effect of chemical reactions and low range of the Peclet number i.e., $4-20$. Recently, Das et al. (2022) employed an unsteady Carreau-Yasuda model to explore

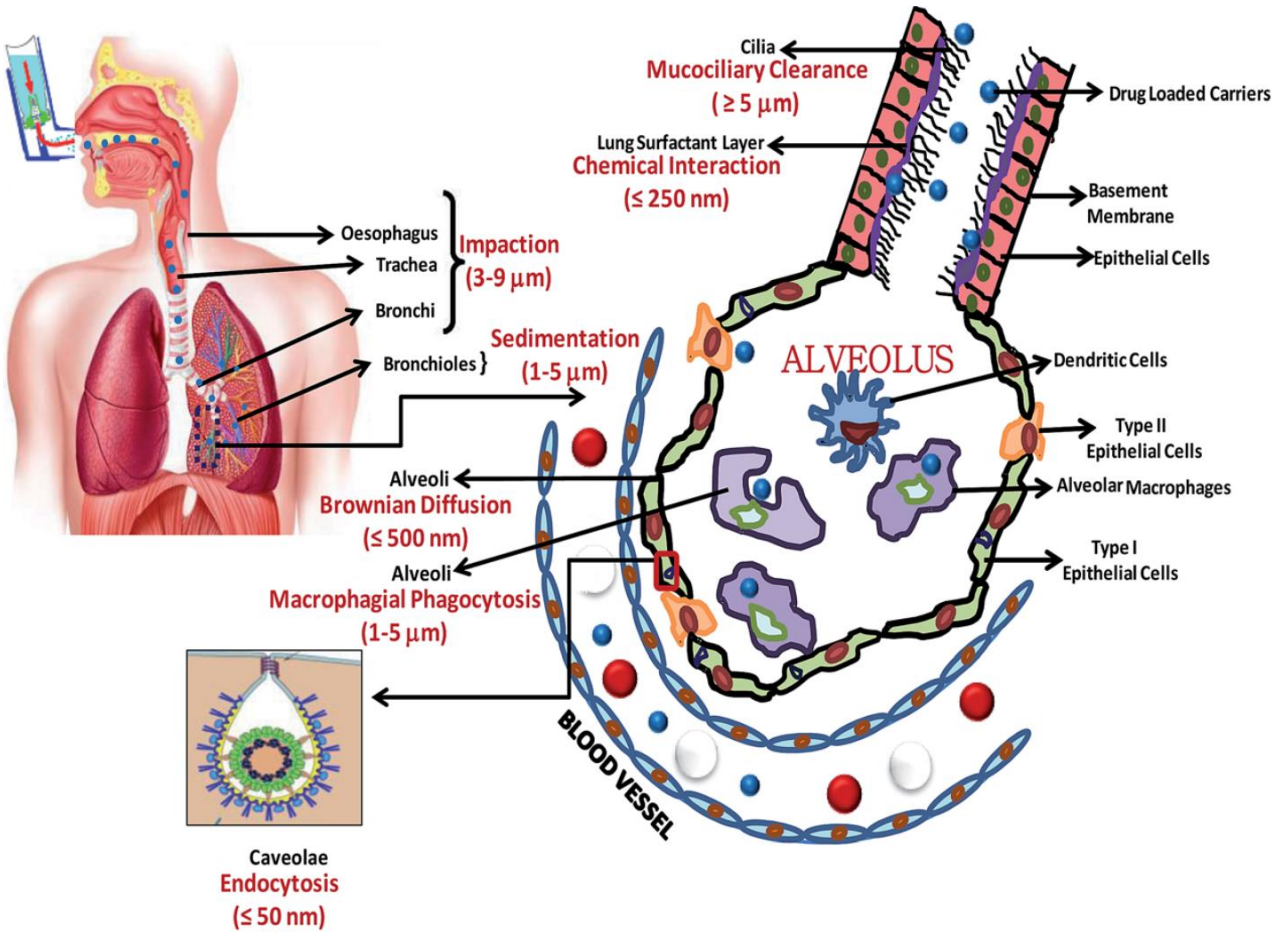

Fig. 1 Pulmonary drug carrier distribution in which the upper left part shows how drug is injected into the human lung, the right part shows the magnified alveoli with the flow of drug through airstream inside the alveolar tube, and the bottom left is the magnified endocytosis. This figure is reprinted from Dhand et al. (2014) with the permission from Royal Society of Chemistry

the dispersion of non-Newtonian blood via a small tube with pulsatile flow and evaluated several coefficients related to fluid transportation between blood and tissues, which can be beneficial in drug delivery in blood arteries.

From these studies we found, various features of the dispersion have been considered, yet the influence of the initially injected solute has remained largely unexplored. This study distinguishes itself in two crucial ways by addressing this factor. Firstly, we compute a time-step constraint to ensure the stability of our proposed numerical scheme, which was not commonly discussed in previous studies. Secondly, we consider the periodic injection of the solute, which has practical applications in pulmonary drug delivery systems. To implement these considerations, we calculated dispersion of a chemically reactive solute injected into a fluid (air, as a mobile phase) flowing through a long circular tube with reversible and irreversible reactions occurring on the tubes' wall (immobile phase). We discretized the advection-diffusion equation by applying an upwind technique with a conservative representation in the diffusion component. To ensure the stability of the proposed numerical scheme, we determined the time step constraint, upholding the maximum principle for the discrete governing equation. As an application of the proposed scheme, we computationally calculated the dispersion of solute across mobile and immobile phases, incorporating periodic injections of the solute, which can be helpful in the development of efficient pulmonary drug delivery systems (Fig. 1). While other results provide insights into the impact of various factors on solute dispersion and chemical reactions.

The section wise organization of the remaining paper is defined as: the advection-diffusion model, non-dimensionalization units, numerical solution technique, and stability analysis are all covered in Section 2. Section 3 provides computational experiments, while Section 4 comprises conclusions.

2. METHODS

2.1 Governing Equations

We consider the fully developed unsteady, incompressible laminar flow of a Newtonian fluid moving through a long, circular tube with radius '$\boldsymbol{a}$' and an axisymmetric velocity field $\boldsymbol{V} = (\boldsymbol{U}, \boldsymbol{W}),$, where $\boldsymbol{U} = \boldsymbol{U}(\boldsymbol{R}, \boldsymbol{Z}, \boldsymbol{T})$ and $\boldsymbol{W} = \boldsymbol{W}(\boldsymbol{R}, \boldsymbol{Z}, \boldsymbol{T})$ are the radial and axial components of the velocity, respectively, and '$\boldsymbol{T}$' represents time. During the flow of fluid, a miscible chemical solute is injected inside the fluid for a very small distance at a very short time. To study the diffusion of the

chemical solute from the mobile (fluid) to immobile (wall tissues) phase, which is reactive at the tube wall, we used a two-dimensional unsteady convection-diffusion model (Ng & Rudraiah, 2008; Kori & Pratibha, 2020, 2022):

$$\frac{\partial \mathrm{C(R,Z,T)}}{\partial \mathrm{T}} + U(\mathrm{R,Z,T})\frac{\partial \mathrm{C(R,Z,T)}}{\partial \mathrm{R}} + W(\mathrm{R,Z,T})\frac{\partial \mathrm{C(R,Z,T)}}{\partial \mathrm{Z}} = D\left[\frac{1}{R}\frac{\partial}{\partial R}\left(\mathrm{R}\frac{\partial \mathrm{C(R,Z,T)}}{\partial \mathrm{R}}\right) + \frac{\partial^2 \mathrm{C(R,Z,T)}}{\partial \mathrm{Z}^2}\right], \quad (1)$$

where $(\mathrm{R,Z,T}) \in \Omega = (0,\mathrm{a}) \times (0,\infty), C(\mathrm{R,Z,T})$ is the concentration of species, and D is the diffusion coefficient of species in the fluid. In Eq. (1) we focused only on complete convection occurring in the axial direction, while complete diffusion takes place in the radial direction. Due to the no slip condition along with the wall, there is no convection in the radial direction, therefore radial velocity becomes zero, $U(R,Z,T) = 0$. While we assume that the axial velocity has the following form due to Poiseuille flow,

$$W(R,Z,T) = 2W_0\left(1 - \frac{R^2}{a^2}\right), \quad (2)$$

where W_0 is the section-mean velocity, which is defined as

$$W_0 = \frac{2}{a^2}\int_0^a WR\, dR. \quad (3)$$

After substituting the above factors in Eq. (1) governing equation converts as

$$\frac{\partial C(R,Z,T)}{\partial T} + 2W_0\left(1 - \frac{R^2}{a^2}\right)\frac{\partial C(R,Z,T)}{\partial Z} = D\left[\frac{1}{R}\frac{\partial}{\partial R}\left(R\frac{\partial C(R,Z,T)}{\partial R}\right) + \frac{\partial^2 C(R,Z,T)}{\partial Z^2}\right]. \quad (4)$$

On the tube wall for $R = a$, two reactions (Ng & Rudraiah, 2008), irreversible (for the part of the solute which is absorbed) and reversible (for the part of solute which is not absorbed by the tube wall and coming back to fluid) are taking place. For simplification these reaction equations are expressed as follows.

For irreversible reaction at $R = a$,

$$\frac{\partial C_s(Z,T)}{\partial T} = -D\frac{\partial C(R,Z,T)}{\partial R} - \Gamma^* C(R,Z,T), \quad (5)$$

For reversible reaction at $R = a$,

$$\frac{\partial C_s(Z,T)}{\partial T} = \kappa\left(\alpha^* C(R,Z,T) - C_s(Z,T)\right), \quad (6)$$

where κ is the reversible phase exchange rate, $C_s(Z,T)$ is the concentration of species absorbed by the tube wall, $\alpha^* = \frac{C_s}{C}$ (Ng & Rudraiah 2008) is the phase partition coefficient, which produced rapid partition when $\alpha^* \leq 1$, otherwise slower partition between the phases. In general, for both reversible and irreversible reactions, α^*should be equal to 0.5.

Furthermore, at $R = 0$ the symmetric boundary condition (Ng and Rudraiah 2008) is defined as

$$\frac{\partial C(R,Z,T)}{\partial R} = 0, \text{or } C = \text{finite} \quad \text{for } R = 0, \quad (7)$$

While the initial condition at $T = 0$ is defined as (Ng & Rudraiah, 2008)

$$C(R,Z,0) = \begin{cases} 1 & \text{if } 0 \leq R \leq a, |Z| \leq Z_s \\ 0 & \text{otherwise} \end{cases}$$

$$C_s(R,Z,0) = 0 \quad \text{for all } Z, \quad (8)$$

where Z_s is the input length of the chemical solute at which a constant concentration of drug (in the case of pulmonary drug delivery system) is released in the banded region ($|Z| \leq Z_s$) as a source. Further, we discussed the periodic injections of the solute in section 3.6.

2.2 Non-Dimensionalization of the Governing Equation

To make the equations dimensionless, we employ the following non-dimensional quantities.

$$c(r,z,t) = \frac{C(R,Z,T)}{C_0}, c_s(r,z,t) = \frac{C_s(Z,T)}{aC_0}, w = \frac{W}{W_0} = 2\left(1 - \frac{R^2}{a^2}\right), r = \frac{R}{a}, z = \frac{Z}{a^2 W_0/D}, t = \frac{T}{a^2/D}, Da = \frac{\kappa a^2}{D}, \alpha = \frac{\alpha^*}{a}, \Gamma = \frac{a\Gamma^*}{D}, Pe = \frac{aW_0}{D}, \quad \ldots\ldots\ldots\ldots \quad (9)$$

where C_0 is the initial concentration. After using the above quantities, Eqs. (4)-(8) are written as follows:

$$\frac{\partial c(r,z,t)}{\partial t} = -2(1-r^2)\frac{\partial c(r,z,t)}{\partial z} + \frac{1}{Pe^2}\frac{\partial^2 c(r,z,t)}{\partial z^2} + \frac{1}{r}\frac{\partial}{\partial r}\left(r\frac{\partial c(r,z,t)}{\partial r}\right), \quad (10)$$

Boundary conditions:

For irreversible reaction,

$$\frac{\partial c_s(r,z,t)}{\partial t} = -\frac{\partial c(r,z,t)}{\partial r} - \Gamma c(r,z,t), \quad r = 1 \quad (11)$$

For reversible reaction,

$$\frac{\partial c_s(r,z,t)}{\partial t} = Da\left(\alpha c(r,z,t) - c_s(r,z,t)\right), \quad r = 1 \quad (12)$$

Symmetric boundary condition:

$$\frac{\partial c(r,z,t)}{\partial r} = 0, r = 0, \quad (13)$$

Initial conditions:

$$c(r,z,0) = \begin{cases} 1 & \text{if } 0 \leq r \leq 1, |z| \leq z_s \\ 0 & \text{otherwise} \end{cases}$$

$$c_s(r,z,0) = 0 \quad \text{for all } z, \quad (14)$$

where Γ denotes the rate of solute absorbed irreversibly by the immobile phase, if $\Gamma \geq 1$, then large amounts of solute are absorbed by the tissue wall in a short time. Da, the Damköhler number indicates how phase exchange takes place. For $Da \geq 1$ the reaction rate is much faster than the diffusion rate (Lau & Ng, 2009; Zhang et al., 2009; Mazumder & Paul, 2012; Debnath et al., 2019, 2020), and Pe is the Peclet number, which expresses the speed at which fluid species are moving and is a ratio of the diffusion rate of species transport to the advection rate. If Pe is high, then the transport of species is influenced by both advection and diffusion. If Pe is low, then the transport of species is dominated by diffusion (Debnath et al., 2019, 2020).

In the current analysis complete axial convection and complete radial diffusion is taking place. So, when the flow is dominated with convection, a sharp gradient is required (a sharp gradient refers to a rapid change in the

quantity being transported over a short distance) to enhance the convective transport and ensure that the transported quantity is efficiently distributed or exchanged within the system. Therefore, we calculated section mean concentration (Saini et al., 2014) of the mobile phase as

$$\bar{c} = 2\int_0^a cr\,dr. \tag{15}$$

In addition, to calculate the axial moment of concentration distribution (Ng & Rudraiah, 2008) we used

$$\mu_n(t) = \int_{-\infty}^{\infty} z^n \bar{c}\,dz \quad (n = 0,1,2,\cdots), \tag{16}$$

here zeroth moment (μ_0) gives the total mass (c_t) of the mobile phase, i.e. $\mu_0 = c_t$, and first moment (μ_1) gives the center of mass of the distribution, i.e. $\mu_1 = \mu_0 c_m(t)$ or $c_m(t) = \frac{\mu_1}{\mu_0}$, while second movement (μ_2) gives variance of the distribution (Ng & Rudraiah, 2008) as follows

$$\sigma^2(t) = \frac{\mu_2}{\mu_0} - c_m^2 \tag{17}$$

We used the Riemann sum formulation to calculate the integrals in Eqs. (15) and (16) so that variance of the distribution in Eq. (17) can be calculated easily.

Further, to accurately measure the dispersion of chemical species, three effective transfer coefficients must be analyzed. The depletion coefficient (D_0) is a measure of the reaction of the solute against the tube wall, the advection coefficient (D_1) is a measure of the velocity of the solute, and the dispersion coefficient (D_2) is a measure of both molecular diffusion and fluid velocity (Sankarasubramanian & Gill, 1973; Ng & Rudraiah, 2008). The relation between total mass (c_t) and time gives the depletion coefficient D_0 (Ng & Rudraiah, 2008)

$$c_t(t) = c_t^0 exp\left(-\int_0^t D_0\,dt\right), \tag{18}$$

where $c_t^0 = 2z_s$ is the initial concentration of solute dissolved in the mobile phase. Then, we can find the advection coefficient D_1 at the center of mass, as the chemical species move according to the advection velocity of the flowing fluid (Ng & Rudraiah, 2008):

$$D_1 = \frac{dc_m}{dt}. \tag{19}$$

Finally, we can obtain the dispersion coefficient D_2 from the change in rate of variance (Ng & Rudraiah, 2008) as

$$D_2 = \frac{1}{2}\frac{d\sigma^2}{dt}. \tag{20}$$

2.3 Numerical Solution Algorithm

To solve the non-dimensional governing equations with boundary conditions, a computational strategy is necessary.

A physical problem using a computational grid with domain Ω_{ik} is depicted in Figure 2. The rectangular cells of the computational grid have sizes of Δr and Δz, and their centers are $(r_i = (i-0.5)\Delta r,\ z_k = (k-0.5)\Delta z)$, where $i = 1,\cdots,N_r$ and $k = 1,\cdots,N_z$. N_r. The number of cells in the r- and z- directions, respectively, are

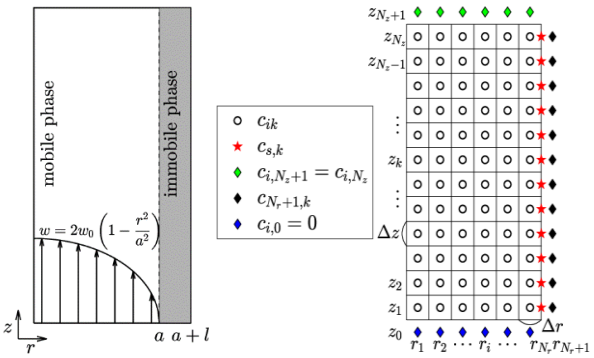

(a) (b)

Fig. 2 Schematic illustration of (a) physical problem and (b) computational grid

N_r and N_z. Diamond symbols (◆, ◆, ◆) are ghost points. Three different color symbols are used for three different boundary conditions. Let $c_{ik}^n = c(r_i, z_k, t_n)$ and $c_{s,k}^n = c_s(z_k, t_n)$, where $t_n = n\Delta t$ and Δt is a time step. The discrete concentration fields c_{ik}^n and $c_{x,k}^n$ are located at cell centers and boundary edges. The completely explicit Euler technique is used in the time-stepping operation. At the start of each time step, provided c_{ik}^n and $c_{s,k}^n$, we want to find c_{ik}^{n+1} and $c_{s,k}^{n+1}$. First, we compute the values at the ghost points. We consider $c_{N_r+1,k}^n$ for $k = 1,\ldots,N_z$. Consider the following equation, which is derived from the boundary conditions defined in Eqs. (11) and (12).

$$-\frac{\partial c}{\partial r} - \Gamma c = Da(\alpha c - c_s). \tag{21}$$

Then, we discretize Eq. (21) as

$$\frac{c_{N_r+1,k}^n - c_{N_r,k}^n}{\Delta r} = -\Gamma\frac{c_{N_r+1,k}^n + c_{N_r,k}^n}{2} - Da\left(\alpha\frac{c_{N_r+1,k}^n + c_{N_r,k}^n}{2} - c_{s,k}^n\right). \tag{22}$$

Equation (22) can rewrite as

$$\left(\frac{1}{\Delta r} + \frac{\Gamma}{2} + \frac{\alpha}{2}Da\right)c_{N_r+1,k}^n = \frac{c_{N_r,k}^n}{\Delta r} - \frac{\Gamma}{2}c_{N_r,k}^n - Da\left(\frac{\alpha}{2}c_{N_r,k}^n - c_{s,k}^n\right). \tag{23}$$

Now, we can obtain the $c_{N_r+1,k}^n$on the ghost points as

$$c_{N_r+1,k}^n = \left[\frac{c_{N_r,k}^n}{\Delta r} - \frac{\Gamma}{2}c_{N_r,k}^n - Da\left(\frac{\alpha}{2}c_{N_r,k}^n - c_{s,k}^n\right)\right] / \left(\frac{1}{\Delta r} + \frac{\Gamma}{2} + \frac{\alpha}{2}Da\right)$$

$$= \left[\left(\frac{1}{\Delta r} - \frac{\Gamma}{2} - \frac{\alpha Da}{2}\right)c_{N_r,k}^n + Dac_{s,k}^n\right] / \left(\frac{1}{\Delta r} + \frac{\Gamma}{2} + \frac{\alpha}{2}Da\right). \quad \ldots\ldots\ldots\ldots\ldots\ldots\ldots\ldots\ldots\ldots \tag{24}$$

In Eq. (24) for the numerical tests, we use the parameters satisfying $(1/\Delta r - \Gamma/2 - \alpha Da/2) \geq 0$. Next, we compute the updated value of $c_{s,k}^{n+1}$ for the next time step update. Let us consider the following equation from Eq. (12)

$$\frac{\partial c_s(z,t)}{\partial t} = Da\big(\alpha c(1,z,t) - c_s(z,t)\big). \tag{25}$$

We discretize Eq. (25) as

$$\frac{c_{s,k}^{n+1}-c_{s,k}^{n}}{\Delta t}=Da\left(\alpha\frac{c_{N_r+1,k}^{n}+c_{N_r,k}^{n}}{2}-c_{s,k}^{n}\right). \tag{26}$$

Rewriting Eq. (26), we have

$$c_{s,k}^{n+1}=c_{s,k}^{n}+\Delta tDa\left(\alpha\frac{c_{N_r+1,k}^{n}+c_{N_r,k}^{n}}{2}-c_{s,k}^{n}\right), \tag{27}$$

which will be used in the next $(n+1)$ −time step update. We apply an explicit Euler method with an upwind method in Eq. (10), such that $c_{ik}^{n+1}\geq 0$:

$$\frac{c_{ik}^{n+1}-c_{ik}^{n}}{\Delta t}+2(1-r_i^2)\frac{c_{ik}^{n}-c_{i,k-1}^{n}}{\Delta z}=\frac{r_{i+\frac{1}{2}}}{r_i}\left(\frac{c_{i+1,k}^{n}-c_{ik}^{n}}{\Delta r^2}\right)-\frac{r_{i-\frac{1}{2}}}{r_i}\left(\frac{c_{ik}^{n}-c_{i-1,k}^{n}}{\Delta r^2}\right)+\frac{c_{i,k+1}^{n}-2c_{ik}^{n}+c_{i,k-1}^{n}}{Pe^2\Delta z^2},\ \text{for } 1\leq i\leq N_r, 1\leq k\leq N_z. \tag{28}$$

We can rewrite Eq. (28) as

$$c_{ik}^{n+1}=c_{ik}^{n}-\Delta t\left[2(1-r_i^2)\frac{c_{ik}^{n}-c_{i,k-1}^{n}}{\Delta z}+\frac{r_{i+\frac{1}{2}}}{r_i}\left(\frac{c_{i+1,k}^{n}-c_{ik}^{n}}{\Delta r^2}\right)-\frac{r_{i-\frac{1}{2}}}{r_i}\left(\frac{c_{ik}^{n}-c_{i-1,k}^{n}}{\Delta r^2}\right)+\frac{c_{i,k+1}^{n}-2c_{ik}^{n}+c_{i,k-1}^{n}}{Pe^2\Delta z^2}\right],\ \text{for } 1\leq i\leq N_r, 1\leq k\leq N_z. \tag{29}$$

We fix the ghost point value at $z=L$ and use zero Neumann boundary condition at $z=H$, i.e., $c_{i,0}^{n}=0, c_{i,N_z+1}^{n}=c_{i,N_z}^{n}$. We note that $r_{1/2}=0$ by definition and $c_{0k}^{n}=c_{1k}^{n}$ by the symmetric condition at $r=0$. Figure 3 shows where the computational domain is placed in the circular tube.

From the above discretization process, we calculate the concentration of solute and then we can calculate section-mean concentration, moments of concentration, and variance of distribution by using Eqs (15), (16) and (17), respectively. After that, we can obtain various transportation coefficients such as the depletion coefficient (D_0), the advection coefficient (D_2), and the dispersion coefficient (D_1) by using the below-defined discretization process

$$D_0^n=\frac{\log c_t^n-\log c_t^{n+1}}{\Delta t},\quad D_1^n=\frac{c_m^{n+1}-c_m^n}{\Delta t},\quad D_2^n=\frac{(\sigma^2)^{n+1}-(\sigma^2)^n}{\Delta t}. \tag{30}$$

Moreover, to obtain phase lock condition we need to follow section 3.6.

2.4 Stability Analysis

In this section, we examine the stability of the proposed numerical scheme to solve the governing equation computationally. Equation (29) can be rewrite as follows:

For $1\leq i\leq N_r$ and $1\leq k\leq N_z$,

$$c_{ik}^{n+1}=\left(1-2(1-r_i^2)\frac{\Delta t}{\Delta z}-\frac{\Delta t}{\Delta r^2}\left(\frac{r_{i+\frac{1}{2}}+r_{i-\frac{1}{2}}}{r_i}\right)-\frac{2\Delta t}{Pe^2\Delta z^2}\right)c_{ik}^{n}+\frac{\Delta t}{\Delta r^2}\left(\frac{r_{i-\frac{1}{2}}}{r_i}\right)c_{i-1,k}+\frac{\Delta t}{\Delta r^2}\left(\frac{r_{i+\frac{1}{2}}}{r_i}\right)c_{i+1,k}+\left(\frac{\Delta t}{Pe^2\Delta z^2}+2(1-r_i^2)\frac{\Delta t}{\Delta z}\right)c_{i,k-1}+\frac{\Delta t}{Pe^2\Delta z^2}c_{i,k+1}. \tag{31}$$

Let us assume $0\leq c_{ik}^{n}\leq 1$, then the following inequality holds by the triangular inequality.

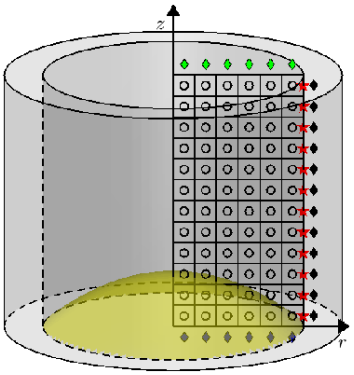

Fig. 3 Schematic of axis symmetric with computational domain

$$c_{ik}^{n+1}\leq\left|1-2(1-r_i^2)\frac{\Delta t}{\Delta z}-\frac{\Delta t}{\Delta r^2}\left(\frac{r_{i+\frac{1}{2}}+r_{i-\frac{1}{2}}}{r_i}\right)-\frac{2\Delta t}{Pe^2\Delta z^2}\right|c_{ik}^{n}+\frac{\Delta t}{\Delta r^2}\left(\frac{r_{i-\frac{1}{2}}}{r_i}\right)c_{i-1,k}+\frac{\Delta t}{\Delta r^2}\left(\frac{r_{i+\frac{1}{2}}}{r_i}\right)c_{i+1,k}+\left(\frac{\Delta t}{Pe^2\Delta z^2}+2(1-r_i^2)\frac{\Delta t}{\Delta z}\right)c_{i,k-1}+\frac{\Delta t}{Pe^2\Delta z^2}c_{i,k+1}. \tag{32}$$

Let us define the maximum value of c_{ik}^{n} on the extended domain with boundary ghost points as

$$c_{\max}^{n}=\max_{\substack{0\leq i\leq N_r+1\\0\leq k\leq N_z+1}}c_{ik}^{n}. \tag{33}$$

Then, from Eq. (32),

$$c_{ik}^{n+1}\leq\left(\left|1-2(1-r_i^2)\frac{\Delta t}{\Delta z}-\frac{\Delta t}{\Delta r^2}\left(\frac{r_{i+\frac{1}{2}}+r_{i-\frac{1}{2}}}{r_i}\right)-\frac{2\Delta t}{Pe^2\Delta z^2}\right|+\frac{\Delta t}{\Delta r^2}\left(\frac{r_{i-\frac{1}{2}}}{r_i}\right)+\frac{\Delta t}{\Delta r^2}\left(\frac{r_{i+\frac{1}{2}}}{r_i}\right)+\left(\frac{\Delta t}{Pe^2\Delta z^2}+2(1-r_i^2)\frac{\Delta t}{\Delta z}\right)+\frac{\Delta t}{Pe^2\Delta z^2}\right)c_{\max}^{n}. \tag{34}$$

Suppose that the following condition is guaranteed.

$$1-2(1-r_i^2)\frac{\Delta t}{\Delta z}-\Delta t\left(\frac{r_{i+\frac{1}{2}}+r_{i-\frac{1}{2}}}{\Delta r^2 r_i}+\frac{2}{Pe^2\Delta z^2}\right)\geq 0. \tag{35}$$

Then, c_{ik}^{n+1} is bounded as

$$0\leq c_{ik}^{n+1}\leq c_{\max}^{n}. \tag{36}$$

The condition (35) can be rewritten as

$$2\Delta t\left(\frac{1-r_i^2}{\Delta z}+\frac{1}{\Delta r^2}+\frac{1}{Pe^2\Delta z^2}\right)\leq 1. \tag{37}$$

Here, $0\leq r_i\leq 1$, therefore, condition (37) is to be as follows:

$$\Delta t\leq 1/\left(\frac{2}{\Delta z}+\frac{2}{\Delta r^2}+\frac{2}{Pe^2\Delta z^2}\right). \tag{38}$$

We should show the values are also bounded at the ghost points: $k=0, k=N_z+1, i=0$, and $i=N_r+1$. Because $c_{i,0}=0, c_{i,N_z+1}=c_{i,N_z}$, and $c_{0,k}=c_{1,k}$, we only consider $c_{N_r+1,k}$ in Eq. (24). Applying explicit Euler method to Eq. (12) we have

$$\frac{c_{s,k}^{n+1}-c_{s,k}^{n}}{\Delta t}=Da\left(\alpha c_{s,k}^{n}-c_{s,k}^{n}\right),$$

$$c_{s,k}^{n+1} = c_{s,k}^{n} + Da\left(\alpha c_{ik}^{n} - c_{s,k}^{n}\right)\Delta t \le c_{s,k}^{n} + Da\left(\alpha - c_{s,k}^{n}\right)\Delta t. \quad (39)$$

In Eq. (39), we can obtain the following time step restriction

$$\Delta t \le \frac{1}{Da}, \quad (40)$$

which assures that $c_{s,k}^{n+1} \le \alpha$, for $n = 0,1,2,\cdots$. Applying the time restriction (40) to Eq. (24), we derive the following inequality.

$$c_{N_r+1,k}^{n} \le \left(\frac{c_{N_r,k}^{n}}{\Delta r} - \frac{\Gamma}{2}c_{N_r,k}^{n} + \frac{\alpha}{2}Da\right) / \left(\frac{1}{\Delta r} + \frac{\Gamma}{2} + \frac{\alpha}{2}Da\right) \quad (41)$$

Because $0 \le c_{N_r,k}^{n} \le 1$, the numerical solution is also bounded on the ghost points $0 \le c_{N_r+1,k}^{n} \le 1$. Therefore, $0 \le c_{max}^{n} \le 1$. From the conditions (38) and (40), we can take time step restriction as

$$\Delta t \le \min\left\{1/\left(\frac{2}{\Delta z} + \frac{2}{\Delta r^2} + \frac{2}{Pe^2}\right), \frac{1}{Da}\right\}. \quad (42)$$

Using Eq. (36), if the time step Δt satisfies the restriction condition (42), the numerical solution c_{ik}^{n+1} is stable and bounded, i.e.,

$$\mathbf{0 \le c_{ik}^{n+1} \le 1}. \quad (43)$$

3. COMPUTATIONAL EXPERIMENTS

In computational experiments we use $z_s = 0.05$ and $Pe = 1000$ throughout the paper.

3.1 Convergence Test

To check the spatial convergence of the numerical solution, we performed the convergence test presented in Fig. 4. Figure 4 shows the concentration of numerical results of $\bar{c}(z)$, $c(0,z)$, and $c(1,z)$ and for various number of grid points N_r and N_z and at $t = 0.1$. In the test, we use a sufficiently small-time step $\Delta t = 0.0001$ in the computational domain $\Omega = (0,1) \times (-0.1,0.9)$. From the result of Fig. 4, the numerical results converge to solid line $(N_r = 50, N_z = 700)$. Therefore, we use grid size $N_r = 50, N_z = 700$ throughout the analysis.

3.2 Comparison Test with the Previous Result

For computational validation of the scheme, we performed a comparison between our results and those in Ng and Rudraiah (2008). Because we do not know exactly what scheme and conditions are used Ng and Rudraiah (2008), hence we collected the data from the figure and performed the comparison between the results produced by the present scheme at grid size $N_r = 50, N_z = 700$ and data of Ng and Rudraiah (2008).

Figure 5 shows the comparison of the area mean concentration $\bar{c}$ of the mobile phase, concentration c at the center $(r = 0)$, and at the wall $(r = 1)$ of the tube, respectively, in Fig. 5 (a), (b), and (c) at time $t = 0.5$, absorption rate $\Gamma = 5$, phase partition number $\alpha = 0.05$, and Damkhöler number $Da = 1$. As shown in the figure all the concentrations first increased with time and after a particular point all the concentrations decreased with time gradually. However, at a very short time, $t = 0.5$, the concentration of the solute at the center of the tube $(c(0,z,0.5))$ has higher values, while at the same time area mean concentration $(\bar{c})$ of the solute inside the mobile phase and concentration at the center of the tube $(c(1,z,0.5))$ have lower values. Physically, early $(t = 0.5)$ the concentration of the solute at the center of the tube is high. At this time, the solute is dispersed throughout the entire area, so less solute reaches the tube wall; therefore, $c(1,z,0.5)$ and $\bar{c}$ are lesser than $c(0,z,0.5)$. The same phenomenon applies to the results of Ng and Rudraiah (2008). Furthermore, as shown in the figure, there is very little difference between the present results and those in Ng and Rudraiah (2008).

Through this analysis, we can say that our scheme and grid size is computationally compatible with the previously published study Ng and Rudraiah (2008).

3.3 Analysis of Various Transport Coefficients

Many researchers (Gill & Sakarasubramanian, 1970; Shankar & Lenhoff, 1991; Ng & Rudraiah, 2008; Das et al., 2021) examined the effect of the transport coefficient. We also shed light on the behavior of time-dependent transport coefficients on solute dispersion for some cases with $\Gamma = 5, 0.5, 0.05, \alpha = 0.05,$ and $Da = 1$.

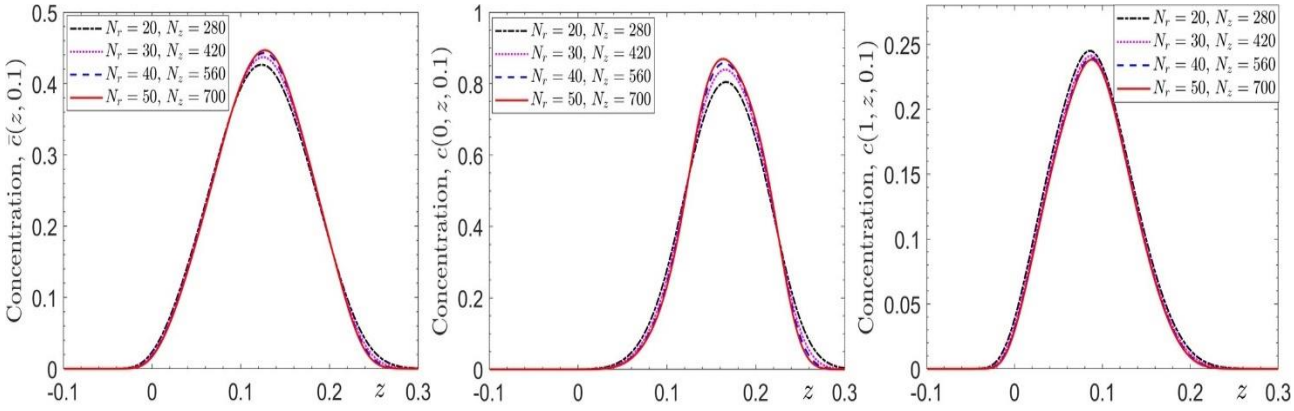

(a) (b) (c)

Fig. 4 Numerical results of (a) $\bar{c}(z, 0.1)$, (b) $c(0, z, 0.1)$, and (c) $c(1, z, 0.1)$ for four cases $N_r = 20, N_z = 280$ (dash-dotted line); $N_r = 30, N_z = 420$ (dotted line); $N_r = 40, N_z = 560$ (dashed line); and $N_r = 50, N_z = 700$ (solid line)

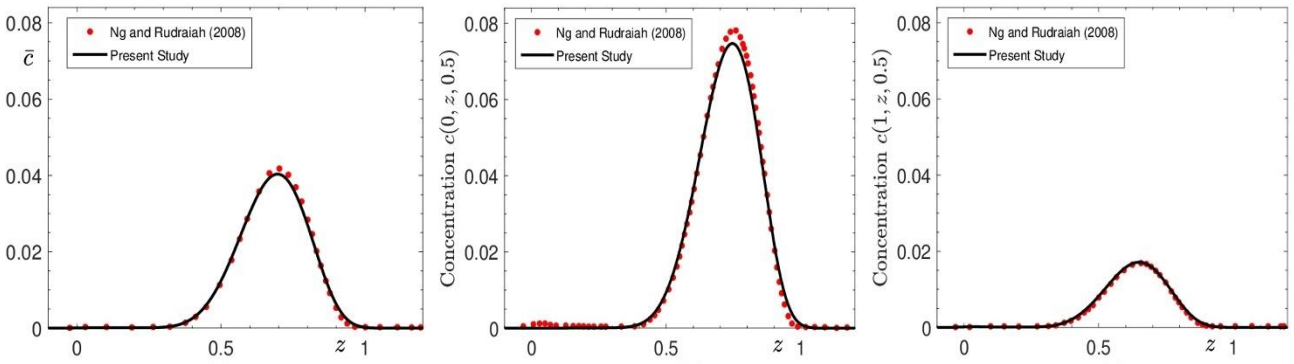

(a) (b) (c)

Fig. 5 Comparison of results produced by present study and Ng and Rudraiah (2008). (a) for area average concentration of mobile phase $(\bar{c})$, (b) concentration c at center $(r = 0)$ and (c) at the wall $(r = 1)$ for $\Gamma = 5, \alpha = 0.05$, and $Da = 1$ at $t = 0.5$

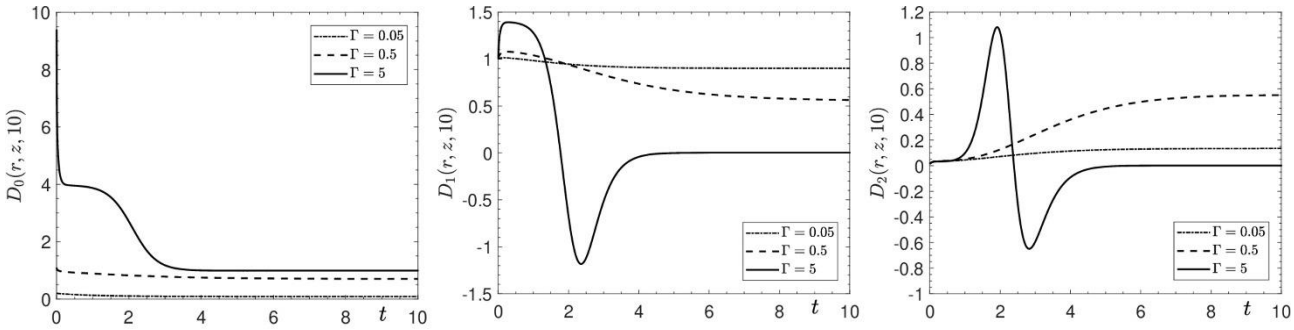

(a) (b) (c)

Fig. 6 (a) Depletion (D_0), (b) advection (D_1), and (c) Dispersion (D_2) of chemical species with different value of absorption rate $\Gamma = 0.05, 0.5, 5$ at $\alpha = 0.005$, and $Da = 1$

Figure 6(a) shows the temporal variation of D_0. At the early stage, values of D_0 are very high for all values of Γ, however, by the time of increasing, it attained a non-transient state after a very long time. The physical implication of this phenomenon is that once the solute is injected, it initially moves at fluid velocity only by convection but after a significant amount of time, solute transport is affected by both solute advection and molecular diffusion. In addition, irreversible wall reactions cause solutes to migrate towards the tube wall where they are consumed and at the tube wall, the solute undergoes a reversible reaction that affects the overall process. However, after a longer period, a stationary equilibrium begins between molecular diffusion and wall reactions. Consequently, increasing the value of Γ depletes more solutes from the system, leading to an increase in D_0. However, the speed at which the solute in the mobile phase is being removed is primarily controlled by the short-term value of D_0 and the transport process stops long before the coefficients reach stable values.

Moreover, the effect of reversible and irreversible reactions on D_1 and D_2 is illustrated in Fig. 6 (b) and (c) in the context of smaller and larger values of Γ. For smaller $\Gamma = 0.05$, a steady state is reached quickly in both D_1 and D_2. However, for $\Gamma = 5$, there is a significant change in D_1 (see Fig. 6 (b), which drops suddenly to a minimum of -0.65), and it gradually stabilizes around zero. Furthermore, the same change is found in D_2, as depicted in Fig. 6 (c), where D_2 coefficient reaches a peak value and then declines sharply before stabilizing at zero.

In the process of phase exchange, negative advection and dispersion can be attributed to a specific condition known as 'back-mixing'. This phenomenon occurs when solutes are absorbed by surfaces or walls within the system and are subsequently released back into the flowing fluid. The delayed release of these solutes can result in their movement against the main flow direction, leading to negative advection and dispersion in the fluid.

3.4 Analysis of Concentration Distribution between Mobile and Immobile Phases with Absorption Rate (Γ)

In this section, we performed an analysis of concentration distribution with area average concentration $(\bar{c})$ distribution in mobile phase, concentration (c) distribution at the center $(r = 0)$ of the tube, and at the wall $(r = 1)$ of the tube together-with concentration distribution in immobile phase (c_s).

For wall absorption we took values from high absorption rate to low absorption rate as $\Gamma = 5, 0.5$, and 0.05 with a fixed value of mobile-immobile phase partitioning number $\alpha = 0.05$ and $Da = 1$ at Pe=1000 then we calculated distribution curves at various time levels $t = 0.1, t = 0.3$, and $t = 0.5$ with two-dimensional and three-dimensional plots. Each figure has five sub figures as shown in Figs. 7-9.

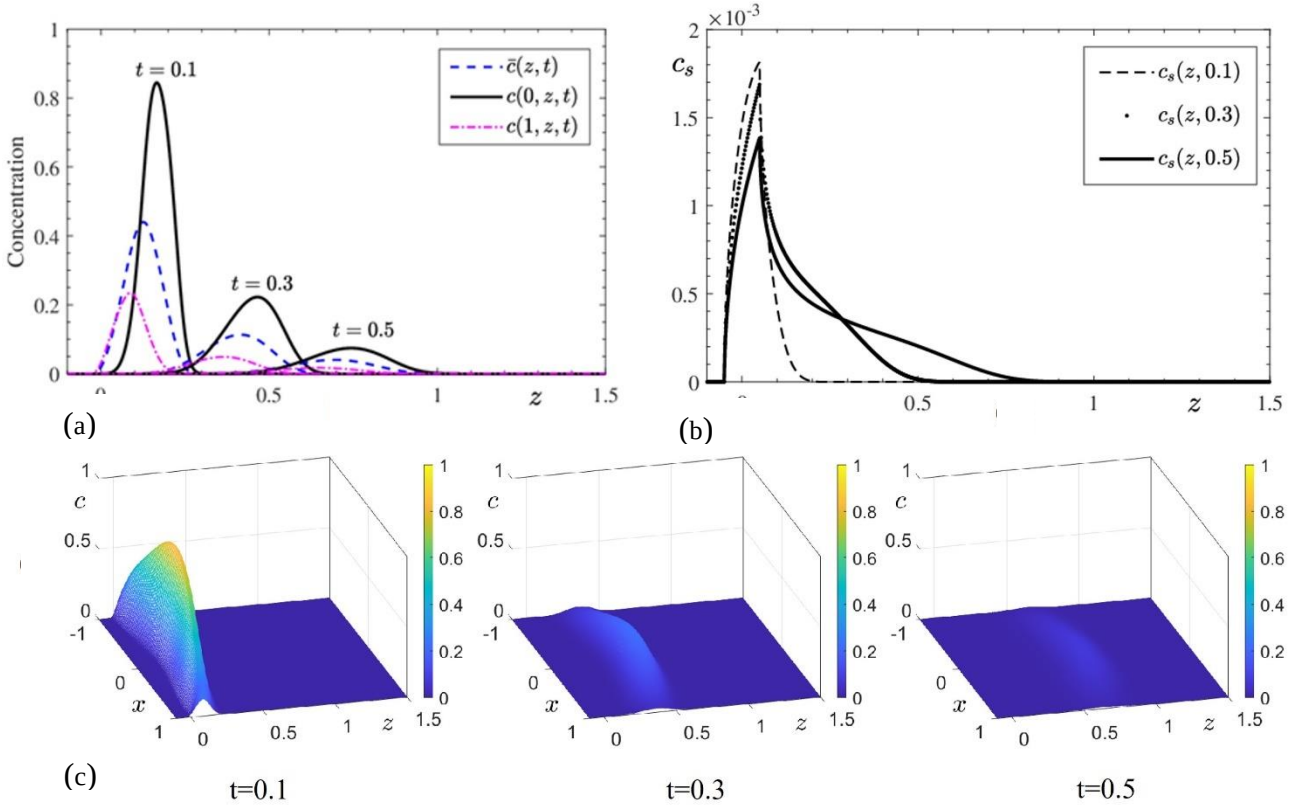

Fig. 7 (a) Area average concentration $(\bar{c})$, together with concentration (c) at center $(r = 0)$ and at the wall $(r = 1)$ for mobile phase, (b) concentration for immobile phase (c_s), and (c) concentration distribution profiles at $t = 0.1$, $t = 0.3$, and $t = 0.5$ for $\Gamma = 5, \alpha = 0.05$, and $Da = 1$

Figure 7 represents distribution of chemical solute for $\Gamma = 5, \alpha = 0.05,$ and $Da = 1$. At very small time, $t = 0.1$, when chemical solute was just injected, the value of concentration was very high at the center of the tube as compared to boundaries of the tube due to advection (see, (a) and axisymmetric subplot (c)) but as time increases gradually up to 0.5 due to diffusion the value of concentration decreases abruptly in the fluid (mobile phase) and absorbed quickly by the tube wall (immobile phase) because the reversible wall retention $(Da = 1)$is not effective, as shown in subplot (b).

While, in Fig. 8 when we decreased the value of $\Gamma = 0.5,$ at $\alpha = 0.05, Da = 1$, we found that the absorption through the immobile phase (see, subplot (b)) was slightly slower than the reversible retention $(Da = 1)$ at the wall, which resulted in solute accumulation on the tube wall over a long period of time and we got quantitatively high value in subplot (b) and a hump on the tube wall (see, subplot (a), and (c). Then, we calculated the distribution of solute inside the fluid and capacity of absorption by the tube wall for a very small absorptionrate $\Gamma = 0.05$ at $\alpha = 0.05,$ and $Da = 1$ in Fig. 9 and found very slow absorption and high retention by the immobile phase. Here, as compared to the above two cases large amount of solute accumulated along the wall and is not absorbed by the tube wall (see, subplot (a), (b)), however, dispersion takes place as time increases (see, subplot (c)).

Hence, the concentration of Figs 8(b) and 9(b) is larger than Fig. 7(b). Physiologically, this analysis shows as soon as we injected the drug inside the tube, if the absorption rate is high then the injected drug will be depleted from fluid and absorbed through the wall in a very short time but if the absorption rate is very low, drug absorption through the tube wall will become down and drug will be accumulated along the walls.

3.5 Concentration Distribution with or Without Reversible and Irreversible Reactions

In this section, we explore how reversible and irreversible phase changes affect the concentration distribution between mobile and immobile phases. Figure 10 (a)-(c) depict the individual effect of Da, α, and Γ respectively, while Fig. 10 (d) illustrates the combined effect of Da, α, and Γ concerning some cases as shown in Table 1. Case 1 is for no reaction, cases 2-4 represents the influence of reversible phase exchange or Da, cases 4 and 7 represents the influence of partition number (α) cases 2 and 6 show the effect of irreversible absorption (Γ).

Figure 10 (a) shows the behavior of phase exchange for $Da = 0, 0.1, 5, 10$ a very small value of $\alpha = 0.005$, and $\Gamma = 0.05$ for $t = 0.5$ on area average concentration distribution of mobile phase. When $Da = 0$, there is no reversible phase exchange was performed and the solute resides inside the mobile phase only; while as Da increased from 0 to 10, the magnitude of the area average concentration decreases as well. This is because as the phase exchange rate increases, more solute moves

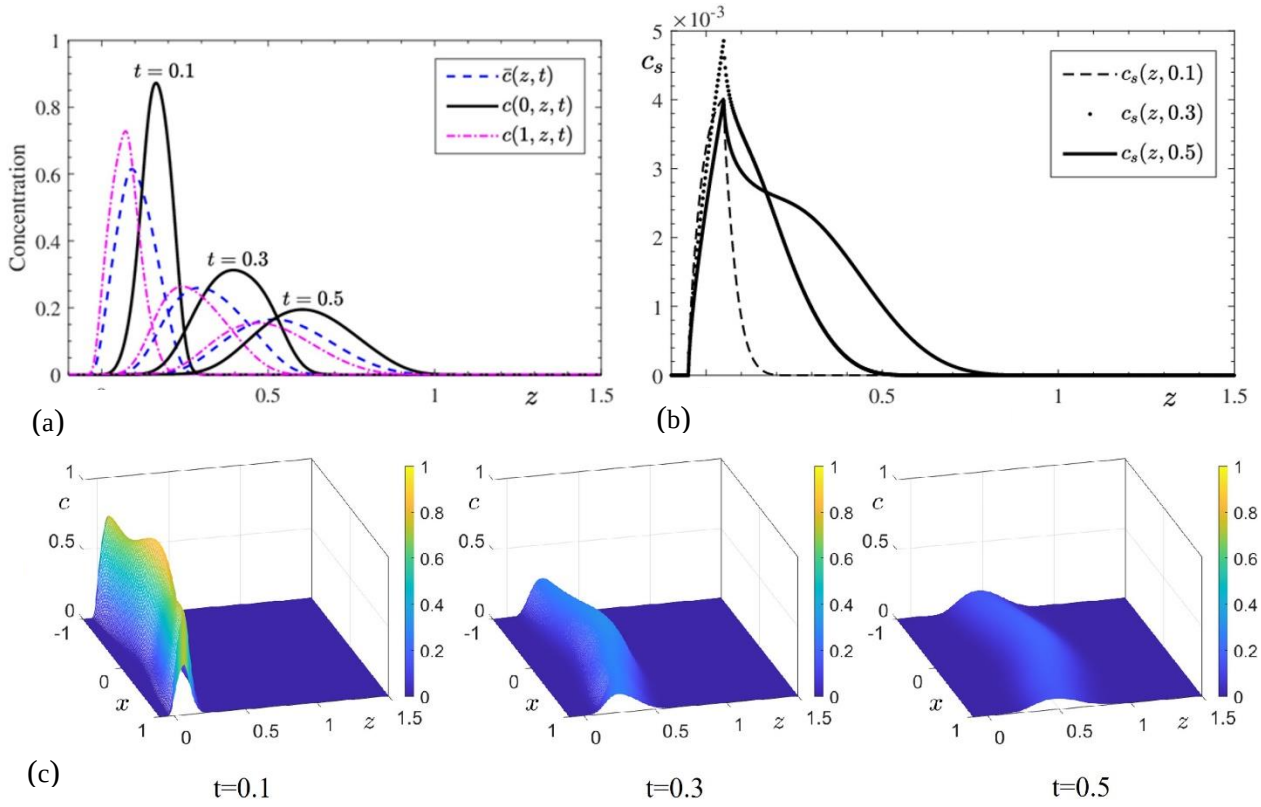

Fig. 8 (a) Area average concentration ($\bar{c}$), together with concentration (c) at center ($r = 0$) and at the wall ($r = 1$) for mobile phase, (b) concentration for immobile phase (c_s), and (c) concentration distribution profiles at $t = 0.1$, $t = 0.3$, and $t = 0.5$ for $\Gamma = 0.5, \alpha = 0.05$, and Da =1

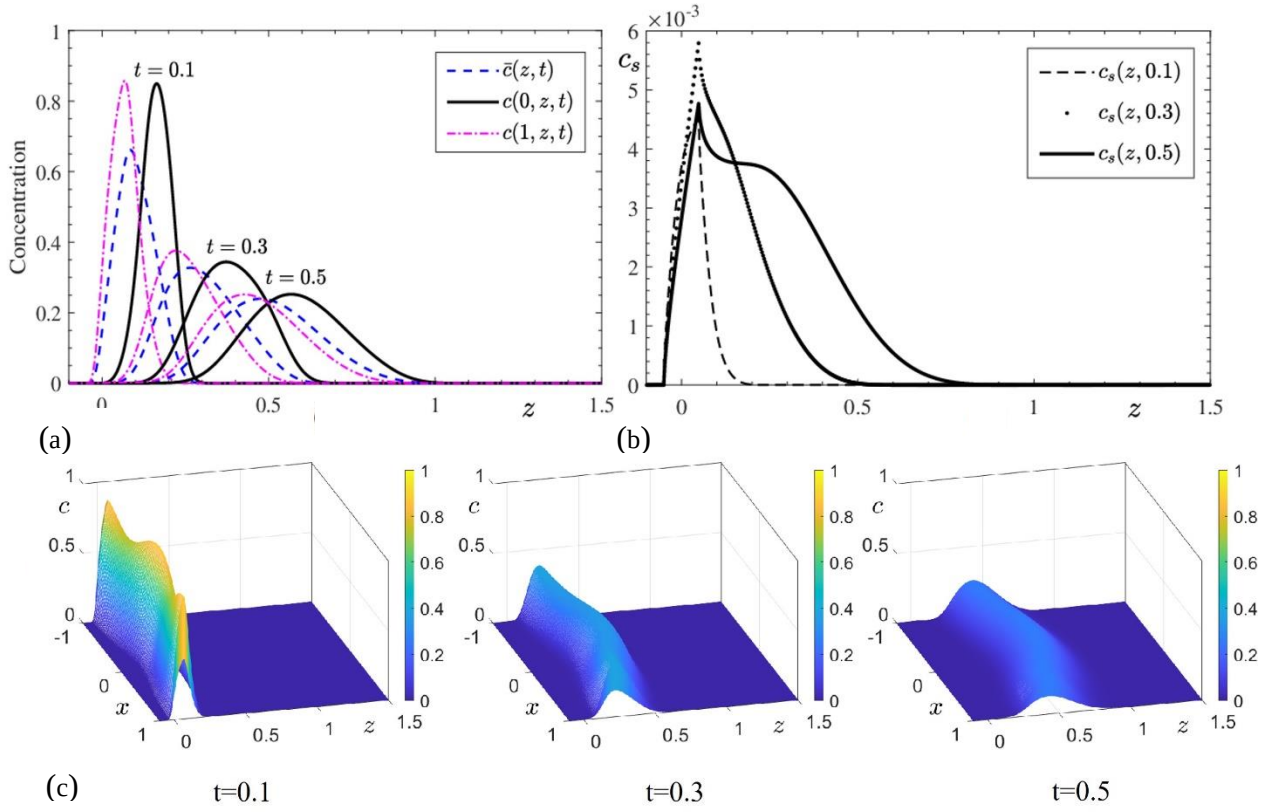

Fig. 9 (a) Area average concentration ($\bar{c}$), together with concentration (c) at center ($r = 0$) and at the wall ($r = 1$) for mobile phase, (b) concentration for immobile phase (c_s), and (c) concentration distribution profiles at $t = 0.1$, $t = 0.3$, and $t = 0.5$ for $\Gamma = 0.05, \alpha = 0.05$, and $Da = 1$

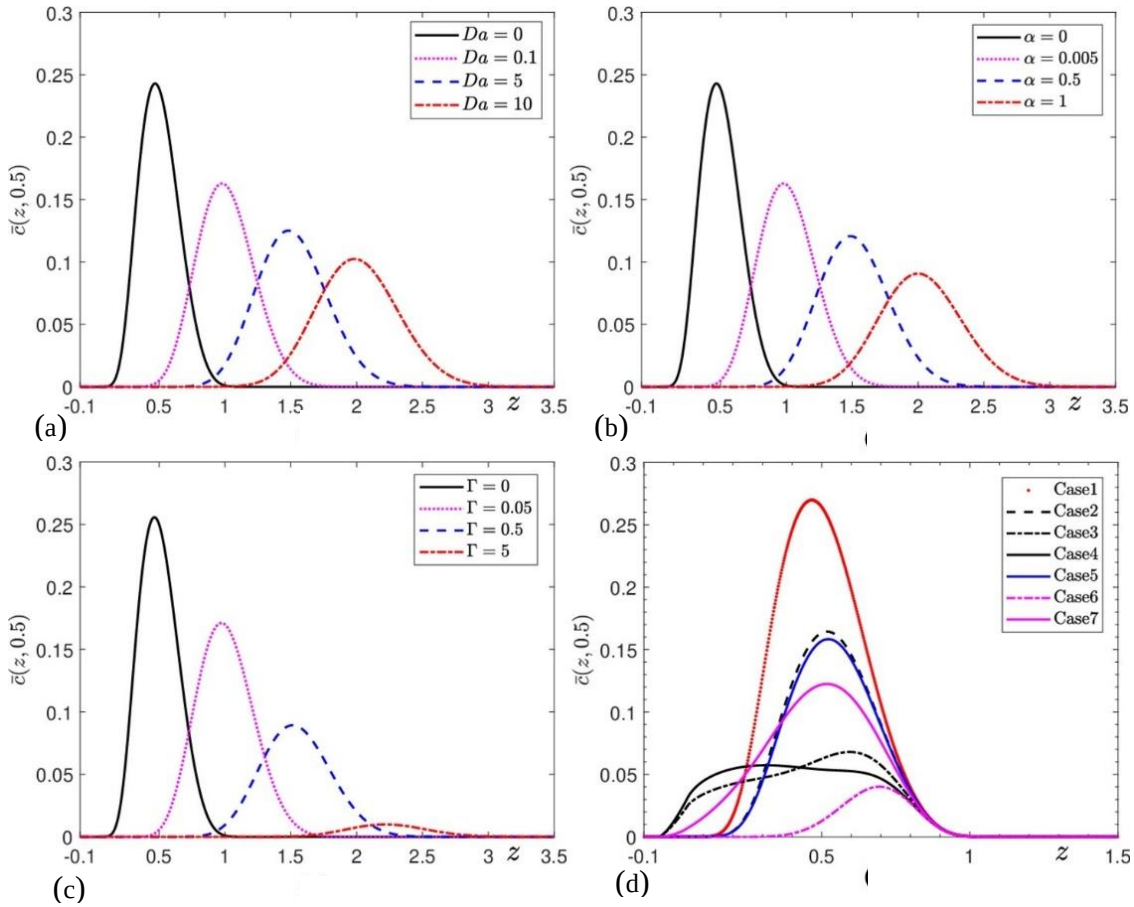

Fig. 10 Area average concentration ($\bar{c}$) of mobile phase for (a) Da = 0, 0.1, 5, 10 at α = 0.005 & Γ = 0.05 (b) α = 0, 0.005, 0.5, 1 at Da = 0.1 & Γ = 0.05, and (c) Γ = 0, 0.05, 0.5, 5 at α = 0.005 & Da = 0.1 together-with (d) Comparison of various cases at t = 0.5

Table 1 Various cases Ng and Rudraiah (2008)used to analyze the distribution of species inside the tube

Cases	Da	α	Γ	Remarks
1	0	0	0	No reaction
2	0.1	0.5	0.5	Slow phase exchange rate
3	5	0.5	0.5	Moderate phase exchanger rate
4	10	0.5	0.5	Fast phase exchange rate
5	0.1	1	0.5	Slow partition between the Phases
6	0.1	0.5	5	Fast absorption rate
7	10	0.1	0.5	Fast partition between the phases

from the mobile phase to the immobile phase then it is absorbed into the tube wall.

After that, the influence of phase partition ratio α on mobile phase area average concentration is shown in Fig. 10 (b) for $\alpha = 0, 0.005, 0.5, 1$ at $Da = 0.1, \Gamma = 0.05,$ and $t = 0.5$. It is illustrated that if $\alpha = 0$ then the impact of only irreversible wall absorption can be seen, and if $\alpha < 0.5$ then most of the cloud remains in the mobile phase and very slow absorption of solute takes place, while if $0.5 < \alpha \leq 1$ then the effect of slow reversible reaction was found since most of the solute is absorbed by immobile phase. While, at equilibrium, both reversible and irreversible reactions proceed with $\alpha = 0.5$. When the value of α is equal to 0.5, the phase exchange mechanism becomes physically faster, which means that the average concentration of the mobile phase will decrease.

Furthermore, the effect of wall absorption rate is calculated on the area average concentration of mobile phase in Fig. 10 (c) for Γ = 0, 0.05, 0.5, 5, at Da = 0.1, α = 0.005, and t = 0.5. We observed, at Γ = 0, only reversible wall retention affects the distribution of concentration. While, as the magnitude of Γ increases up to 5 (0 < Γ < 5) significant value of concentration is maintained by the mobile phase, but after that as the magnitude of Γ increases (Γ ≥ 5) the concentration cloud drops abruptly. The reason behind this phenomenon is, as soon as the solute is injected into the fluid flow, it flies with the velocity of fluid by the act of advection and reaches the tube wall where due to diffusion it performs chemical reaction with the tube wall. The physical significance of this result is that the large amount of solute comes back to the mobile phase if absorption through the tube wall is slow, while reduction of solute is found inside the mobile phase for a large absorption rate.

Furthermore, Fig. 10(d) depicted the axial distribution of the solute in mobile phase for seven different conditions. As shown in Fig. 10, case 1 is no reaction case. For cases 1, 2 and 5-7 the distribution curve is a single peak, while the additional peak has emerged in cases 3, and 4, also area under the curve is significantly decreased in cases 3, 4, and 6 due to high reversible phase exchange (Da) and irreversible absorption rate (Γ), respectively

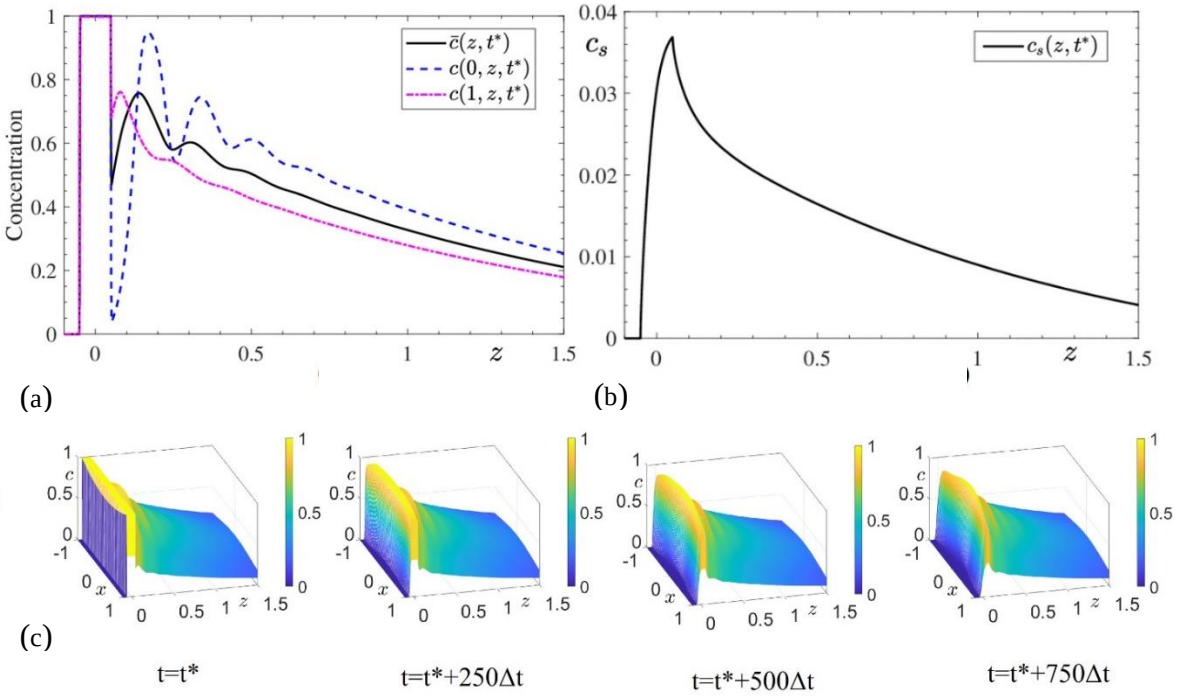

Fig. 11 Results for $1000\,\Delta t$ periodic injections. (a) Area average concentration $(\bar{c})$, together with concentration (c) at center $(r = 0)$ and at the wall $(r = 1)$ for mobile phase, (b) concentration for immobile phase (c_s), and (c) concentration distribution profiles at $t = t^*, t = t^* + 250\Delta t, t = t^* + 500\Delta t$, and $t = t^* + 750\Delta t$

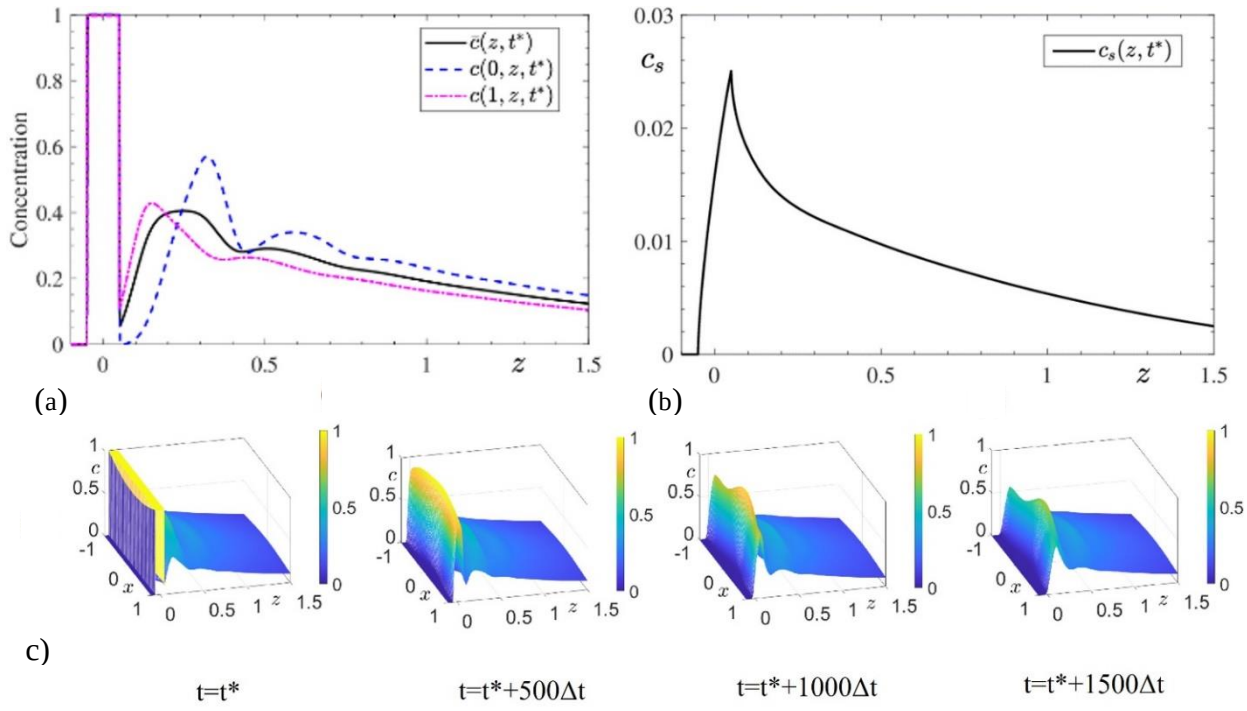

Fig. 12 Results for $2000\,\Delta t$ periodic injections. (a) Area average concentration $(\bar{c})$, together with concentration (c) at center $(r = 0)$ and at the wall $(r = 1)$ for mobile phase, (b) concentration for immobile phase (c_s), and (c) concentration distribution profiles at $t = t^*, t = t^* + 500\Delta t, t = t^* + 1000\Delta t$, and $t = t^* + 1500\Delta t$

Also, in cases 4 both the reversible and irreversible reactions are took place at α = 0.5; while in cases 5 and 7 value of α is 1 and 0.1 which cause either irreversible reaction or reversible, respectively. Physiologically, it is noted that for a high magnitude absorption rate long time dispersion will not be obtained since the mass is depleted by the immobile phase very fast.

3.6 Periodic Injection

For periodic injection we used the diffusion model (Ng & Rudraiah, 2008; Kori & Pratibha, 2020, 2022) as defined in Eq. (10) with the periodic injection condition as

$$c(r,z,t) = 1, \text{if } 0 \le r \le 1, |z| \le z_s, \tag{44}$$

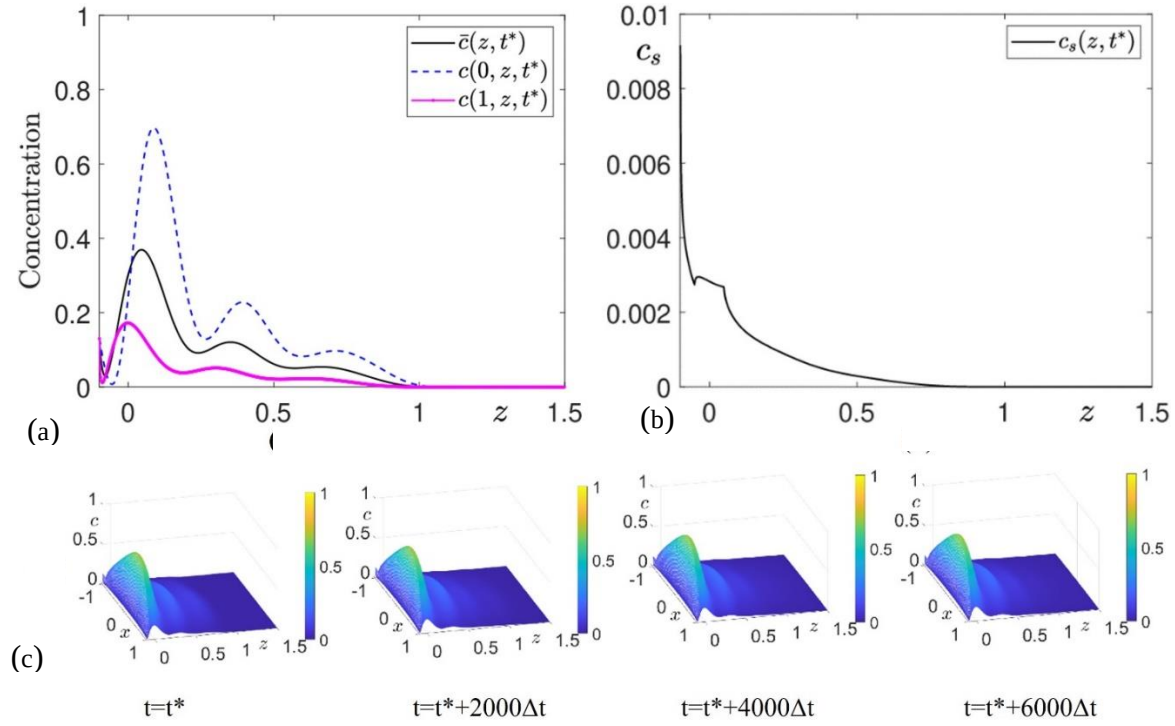

Fig. 13 Results for periodic injections condition: Eq. (45). (a) Area average concentration $(\bar{c})$, together with concentration (c) at center $(r = 0)$ and at the wall $(r = 1)$ for mobile phase, (b) concentration for immobile phase (c_s), and (c) concentration distribution profiles at $t = t^*, t = t^* + 2000\Delta t, t = t^* + 4000\Delta t$, and $t = t^* + 6000\Delta t$

where z_s is the input length of the constant concentration of the chemical solute or drug where the source at the banded region is located initially and taken as $z_s = 0.05$ in this paper; and $t = nP$ with some periodic cycle $P = 1000\Delta t$ for $n = 0,1,2,\cdots$. Then, we investigated the effects of periodic injections. The periodic injections make a phase-lock phenomenon, where the dynamics repeat periodically. We perform the simulations on computational domain $(0,1) \times (-0.1,1.5)$ with parameters as $\Gamma = 0.5, Da = 1,$ and $\alpha = 0.05$. Subplots (a) and (b) of Figs. 11 and 12 show one cycle snapshots of dynamics with $1000\Delta t$ and $2000\Delta t$ periodic injections, respectively. In the following tests, we set $t^* = 20000\Delta t$, which is the phase-lock state. Subplot (c) of Figs. 11 and 12 show concentration distribution profiles concerning periodic injection from $t = 0.1$ to $t = 1.5$, for each injection concentration increases under the condition $c \leq 1$ and diffuses between mobile and immobile phases. However, at time $t = 1.5$ after injection of chemical solute, less amount of concentration is distributed, and this is a breakthrough condition just before phase lock. Furthermore, we adopted the following source using continuous periodic injection inside the domain near the boundary $z = L$:

$$c(r,z,t) = 0.5(1 + \cos(10\pi t)), 0 \leq r \leq 1, z = -0.1 + \Delta z. \quad (45)$$

We set a phase-lock state at $t^* = 15000\Delta t$ and obtained the results with a new injection condition as shown in Fig. 13. Subplots (a) and (b) of Fig. 13 is the dynamics for concentration distribution at $t^* = 5235\Delta t$, while subplot (c) of Fig. 13 shows concentration distribution profiles of some random time periods. For each injection concentration increases under the condition as given in Eq. (45) and diffuses between mobile and immobile phases. However, by using the cosine condition we observed that the increment in concentration is not as high as with the previous condition. Moreover, the distribution of solute between the phases is also very low. Such computer simulations are useful in drug delivery systems that require periodic injections of the drug.

4. CONCLUSION

In this article, we investigated the effect of a chemical solute, injected over a short distance for a very brief time, on flux transportation between mobile and immobile phases of a long circular tube. For the governing equation of fluid flowing inside the tube, we used the advection-diffusion equation, while on the wall of the tube, we used phase exchange boundary conditions which consist of an irreversible reaction caused by absorption and a reversible reaction caused by phase exchange. The equation of diffusion with boundary conditions is solved numerically. The primary goal of this research is to determine the stability criteria of a finite difference numerical scheme connected to time step, as well as to conduct a computational investigation of periodic injections. Also, we compared our work with the previous work (Ng & Rudraiah, 2008) and found result produced by our scheme is compatible with the existing literature with better performance, more accuracy, and greater stability. From the numerical computation we can draw the following conclusions.

- We investigated how fluid properties and reaction kinetics affected the transport of solutes. The irreversible absorption parameter ($\boldsymbol{\Gamma}$) and the diffusion coefficient ($\boldsymbol{D_0}$), which results in a quasi-steady state for high $\boldsymbol{t}$ and $\boldsymbol{\Gamma}$, were shown to have a positive association. Also, because of a higher advection velocity in the center of the tube, the advection coefficient ($\boldsymbol{D_1}$) increased as $\boldsymbol{\Gamma}$ increased. Yet, the diffusive coefficient ($\boldsymbol{D_2}$) decreased over time with increasing $\boldsymbol{\Gamma}$ because of a low-velocity gradient in the intermediate region.
- We calculated the dispersion of concentration with different values of absorption rate at various time levels. We found that for a high absorption rate chemical solute was absorbed by the tube wall very fast and less amount of fluid accumulated at the tube wall, while for the low value of absorption rate chemical solute was not absorbed by the tube wall and a large amount of solute accumulated along the tube wall. We conclude from this behavior that for a large value of absorption rate, irreversible reaction dominates reversible reaction; and for the low value of absorption rate, reversible reaction dominates irreversible reaction.
- We analyzed the condition for periodic injection of chemical solute inside a tube for some cycle of time. From that, we found that after some cycles of time, the concentration profile is phase locked. The steady state with cosine condition is achieved much earlier as compared to the previous condition.
- In area average concentration distribution, the presence of a high Damköhler number ($\boldsymbol{Da \geq 1}$) will limit the second peak in different cases. If the rate of phase exchange is less effective ($\boldsymbol{Da \leq 1}$), accessing the long-term distribution takes more time. However, quick distribution can be observed under specific conditions, such as a high Damköhler number ($\boldsymbol{Da \geq 10}$) and a high absorption rate ($\boldsymbol{\Gamma > 0.5}$). These quick distributions can provide valuable insights into the early development of dispersion in various situations.

Overall, our study contributes to the understanding of solute dispersion in complex systems and proposes a stable and accurate numerical method for solving the governing equations. The consideration of periodic injections and the introduction of a time-step constraint are novel aspects of our work. Through analysis of area average concentration distribution, numerical results can be obtained that can be used to determine the optimal frequency of injection for pulmonary drug delivery systems. By injecting the drug at the right frequency, the drug can be delivered effectively and efficiently, resulting in better treatment outcomes. Moreover, in our future research, we will investigate the porosity of the immobile layer, a consideration not included in our current model.

ACKNOWLEDGMENTS

Jyoti (the first author) is supported by the Brain Pool program, which is financed by the Ministry of Science and ICT via the National Research Foundation of Korea (2022H1D3A2A02081237). J.S. Kim (corresponding author) is funded by the National Research Foundation (NRF) of Korea through the project BK21 FOUR.

CONFLICT OF INTEREST

No potential conflict of interest was reported by the authors.

AUTHORS CONTRIBUTION

Jyoti: Conceptualization, Software, Validation, Visualization, Writing - Original Draft, Investigation. **Soobin Kwak**: Software, Formal analysis, Investigation, Visualization. **Seokjun Ham**: Methodology, Software, Validation, Formal analysis, Visualization. **Junseok Kim**: Conceptualization, Methodology, Validation, Formal analysis, Writing - Review & Editing, Supervision, Project administration, Funding acquisition

REFERENCES

Ani, E. C., Wallis, S., Kraslawski, A., & Agachi, P. S. (2009). Development, calibration and evaluation of two mathematical models for pollutant transport in a small river. *Environmental Modelling & Software*, *24*(10), 1139–1152. https://doi.org/10.1016/j.envsoft.2009.03.008

Aris, R. (1956). On the dispersion of a solute in a fluid flowing through a tube. *Proceedings of the Royal Society of London. Series A. Mathematical and Physical Sciences*, *235*(1200), 67–77. https://doi.org/10.1016/S1874-5970(99)80009-5

Abidin, S. N. A. M. Z., Jaafar, N. A., & Ismail, Z. (2021). Herschel-Bulkley model of blood flow through a stenosed artery with the effect of chemical reaction on solute dispersion. *Malaysian Journal of Fundamental and Applied Sciences*, *17*(4), 457–474. https://doi.org/10.11113/mjfas.v17n4.2144

Barati, P., & Saghafian, M. (2022). Optimum geometric bifurcation under pulsating flow assuming minimum energy consumption in cardiovascular system, an extension on murray's law. *Journal of Applied Fluid Mechanics*, *15*(3), 687–695. https://doi: 10.47176/jafm.15.03.33190

Bég, O. A., & Roy, A. K. (2022). Moment analysis of unsteady bi-component species (drug) transport with coupled chemical reaction in non-Newtonian blood flow. *Chinese Journal of Physics*, *77*, 1810–1826. https://doi.org/10.1016/j.cjph.2022.04.003

Ben-Tal, A. (2006). Simplified models for gas exchange in the human lungs. *Journal of theoretical biology*, *238*(2), 474–495. https://doi.10.1016/j.jtbi.2005.06.005

Bel Hadj Taher, A., Kanfoudi, H., & Zgolli, R. (2022). numerical prediction approach of cavitation erosion based on 3D simulation flow. *Journal of Applied Fluid Mechanics*, *15*(4), 1165–1177. https://doi:

10.47176/jafm.15.04.1016

Chatwin, P. C. (1970). The approach to normality of the concentration distribution of a solute in a solvent flowing along a straight pipe. *Journal of Fluid Mechanics*, *43*(2), 321–352. https://doi.10.1017/S0022112070002409

Das, P., Sarifuddin, S., Rana, J., & Mandal, P. K. (2021). Solute dispersion in transient Casson fluid flow through stenotic tube with exchange between phases. *Physics of Fluids*, *33*(6). https://doi.org/10.1063/5.0052770

Das, P., Sarifuddin, Rana, J., & Kumar Mandal, P. (2022). Unsteady solute dispersion in the presence of reversible and irreversible reactions. *Proceedings of the Royal Society A*, *478*(2264), 20220127. https://doi.10.1098/rspa.2022.0127

Debnath, S., Saha, A. K., Siddheshwar, P. G., & Roy, A. K. (2019). On dispersion of a reactive solute in a pulsatile flow of a two-fluid model. *Journal of Applied Fluid Mechanics*, *12*(3), 987–1000. https://doi.org/10.29252/jafm.12.03.29101

Debnath, S., Saha, A. K., Mazumder, B. S., & Roy, A. K. (2020). On transport of reactive solute in a pulsatile Casson fluid flow through an annulus. *International Journal of Computer Mathematics*, *97*(11), 2303-2319. https://doi.org/10.1080/00207160.2019.1695047

Davidson, M. R., & Schroter, R. C. (1983). A theoretical model of absorption of gases by the bronchial wall. *Journal of Fluid Mechanics*, *129*, 313–335. https://doi.10.1017/S0022112083000786

Dhand, C., Prabhakaran, M. P., Beuerman, R. W., Lakshminarayanan, R., Dwivedi, N., & Ramakrishna, S. (2014). Role of size of drug delivery carriers for pulmonary and intravenous administration with emphasis on cancer therapeutics and lung-targeted drug delivery. *RSC advances*, *4*(62), 32673–32689. https://doi.org/10.1039/C4RA02861A

Fu, X., Gao, R., & Wu, Z. (2016). Additional longitudinal displacement for contaminant dispersion in wetland flow. *Journal of Hydrology*, *532*, 37–45. https://doi.org/10.1016/j.jhydrol.2015.10.064

Gill, W. N., & Sankarasubramanian, R. (1970). Exact analysis of unsteady convective diffusion. *Proceedings of the Royal Society of London. A. Mathematical and Physical Sciences*, *316*(1526), 341–350. https://doi.org/10.1098/rspa.1970.0083

Giddings, J. C., & Eyring, H. (2002). A molecular dynamic theory of chromatography. *The Journal of Physical Chemistry*, *59*(5), 416–421. https://doi.10.1021/J150527A009

Ibrahim, A., Meyrueix, R., Pouliquen, G., Chan, Y. P., & Cottet, H. (2013). Size and charge characterization of polymeric drug delivery systems by Taylor dispersion analysis and capillary electrophoresis. *Analytical and bioanalytical chemistry*, *405*, 5369–5379. https://doi.10.1007/s00216-013-6972-4

Jiang, W., Zeng, L., Fu, X., & Wu, Z. (2022). Analytical solutions for reactive shear dispersion with boundary adsorption and desorption. *Journal of Fluid Mechanics*, *947*, A37. https://doi.10.1017/jfm.2022.656.

Jiang, Y., & Grotberg, J. B. (1993). Bolus contaminant dispersion in oscillatory tube flow with conductive walls. https://doi.10.1115/1.2895507

Kori, J. (2020). Effect of first order chemical reactions on the dispersion coefficient associated with laminar flow through fibrosis affected lung. *Journal of biomechanics*, *99*, 109494. https://doi.10.1016/j.jbiomech.2019.109494

Kori, J., & Pratibha. (2022). Effect of first order chemical reactions through tissue-blood interface on the partial pressure distribution of inhaled gas. *Computer Methods in Biomechanics and Biomedical Engineering*, *25*(1), 84–96. https://doi.10.1080/10255842.2021.1932839

Lau, M. W., & Ng, C. O. (2009). *On the early development of dispersion in flow through a tube with wall reactions.* In New Trends in Fluid Mechanics Research: Proceedings of the Fifth International Conference on Fluid Mechanics (Shanghai, 2007), Springer Berlin Heidelberg. https://doi.org/10.1007/978-3-540-75995-9_224

Le, A. D., & Tran, H. T. (2022). Improvement of mass transfer rate modeling for prediction of cavitating flow. *Journal of Applied Fluid Mechanics*, *15*(2), 551-561. https://doi: 10.47176/jafm.15.02.33231

Mazumder, B. S., & Paul, S. (2012). Dispersion of reactive species with reversible and irreversible wall reactions. *Heat and Mass Transfer*, *48*, 933–944. https://doi.org/10.1007/s00231-011-0920-7

Mazumder, B. S., & Das, S. K. (1992). Effect of boundary reaction on solute dispersion in pulsatile flow through a tube. *Journal of Fluid Mechanics*, *239*, 523-549.

https://doi.org/10.1017/S002211209200452X

Mohseni, M., & Domfeh, M. K. (2023). Numerical analysis of transient vortex formation at the outlet of a tank containing gas-liquid phases. *Journal of Applied Fluid Mechanics*, *16*(11), 2235–2248. https://doi: 10.47176/jafm.16.11.1942

Ng, C. O., & Rudraiah, N. (2008). Convective diffusion in steady flow through a tube with a retentive and absorptive wall. *Physics of Fluids*, *20*(7). https://doi.10.1063/1.2958322

Paramanantham, S. S. S., Nagulapati, V. M., & Lim, H. (2022). Numerical investigation of the influence of microchannel geometry on the droplet generation process. *Journal of Applied Fluid Mechanics*, *15*(5), 1291–1305. https://doi: 10.47176/jafm.15.05.1126

Rana, J., & Murthy, P. V. S. N. (2016). Solute dispersion in pulsatile Casson fluid flow in a tube with wall absorption. *Journal of Fluid Mechanics*, *793*, 877–

914. https://doi.10.1017/jfm.2016.155

Rana, J., & Murthy, P. V. S. N. (2017). Unsteady solute dispersion in small blood vessels using a two-phase Casson model. *Proceedings of the Royal Society A: Mathematical, Physical and Engineering Sciences*, *473*(2204), 20170427. https://doi.10.1098/rspa.2017.0427

Roy, A. K., & Bég, O. A. (2021). Mathematical modelling of unsteady solute dispersion in two-fluid (micropolar-Newtonian) blood flow with bulk reaction. *International Communications in Heat and Mass Transfer*, *122*, 105169. https://doi.org/10.1016/j.icheatmasstransfer.2021.105169

Shaw, S., Ganguly, S., Sibanda, P., & Chakraborty, S. (2014). Dispersion characteristics of blood during nanoparticle assisted drug delivery process through a permeable microvessel. *Microvascular Research*, *92*, 25–33. https://doi.10.1016/j.mvr.2013.12.007

Saini, A., Katiyar, V. K., & Pratibha. (2014). Effects of first-order chemical reactions on the dispersion coefficient associated with laminar flow through the lungs. *International Journal of Biomathematics*, *7*(02), 1450021. https://doi.10.1142/S1793524514500211

Sankarasubramanian, R., & Gill, W. N. (1973). Unsteady convective diffusion with interphase mass transfer. *Proceedings of the Royal Society of London. A. Mathematical and Physical Sciences*, *333*(1592), 115–132. https://doi.10.1098/rspa.1973.0051

Shankar, A., & Lenhoff, A. M. (1991). Dispersion and partitioning in short coated tubes. *Industrial & engineering chemistry research*, *30*(5), 828–835. https://doi.10.1016/j.jtbi.2005.06.005.

Taylor, G. I. (1953). Dispersion of soluble matter in solvent flowing slowly through a tube. *Proceedings of the Royal Society of London. Series A. Mathematical and Physical Sciences*, *219*(1137), 186–203. https://doi.org/10.1098/rspa.1953.0139

Venditti, C., Giona, M., & Adrover, A. (2022). Exact moment analysis of transient/asymptotic dispersion properties in periodic media with adsorbing/desorbing walls. *Physics of Fluids*, *34*(12). https://doi.10.1063/5.0130648

Wang, Y. F., & Huai, W. X. (2019). Random walk particle tracking simulation on scalar diffusion with irreversible first-order absorption boundaries. *Environmental Science and Pollution Research*, *26*, 33621–33630. https://doi.org/10.1007/s11356-019-06422-1

Wu, Z., Zeng, L., Chen, G. Q., Li, Z., Shao, L., Wang, P., & Jiang, Z. (2012). Environmental dispersion in a tidal flow through a depth-dominated wetland. *Communications in Nonlinear Science and Numerical Simulation*, *17*(12), 5007–5025. https://doi.org/10.1016/j.cnsns.2012.04.006

Wu, Z., & Chen, G. Q. (2014). Approach to transverse uniformity of concentration distribution of a solute in a solvent flowing along a straight pipe. *Journal of Fluid Mechanics*, *740*, 196–213. https://doi.10.1017/jfm.2013.648

Wu, Z., Zhou, D., Li, S., Yang, J., Chen, G., & Li, X. (2022). Numerical Analysis of the Effect of Streamlined Nose Length on Slipstream of High-Speed Train Passing through a Tunnel. *Journal of Applied Fluid Mechanics*, *15*(6), 1933–1945. https://doi.org/10.47176/jafm.15.06.1189

Yang, X., Hu, Y., Gong, Z., Jian, J., & Liu, Z. (2021). Numerical study of combined drag reduction bases on vortex generators and riblets for the ahmed body using IDDES methodology. *Journal of Applied Fluid Mechanics*, *15*(1), 193–207. https://doi:10.47176/jafm.15.01.32832

Zhang, D. X., Lu, Z. M., Liu, Y. L., & Chiu-On, N. G. (2009). Numerical simulation of the dispersion in oscillating flows with reversible and irreversible wall reactions. *Journal of Hydrodynamics, Ser. B*, *21*(4), 482-490. https://doi.org/10.1016/S1001-6058(08)60174-2